RSC Advances

Sorption of Lead from Aqueous Solutions by a Commercially Available Tungsten Trioxide Nanopowder

Journal:	*RSC Advances*
Manuscript ID:	RA-ART-06-2015-011299.R1
Article Type:	Paper
Date Submitted by the Author:	05-Aug-2015
Complete List of Authors:	Apblett, Allen; Oklahoma State University, Chemistry Perkins, Cory; Oklahoma State University, Chemistry Reed, Travis; Oklahoma State University, Chemistry

Environmental Science: Nano

ARTICLE

Sorption of Lead from Aqueous Solutions by a Commercially Available Tungsten Trioxide Nanopowder

Received 00th January 20xx,
Accepted 00th January 20xx

DOI: 10.1039/x0xx00000x

www.rsc.org/

*Cory K. Perkins, Travis M. Reed, and Allen W. Apblett**

A commercially-available tungsten trioxide nanopowder was investigated and shown to be an excellent sorbent for Pb^{2+} ions in water. The sorption kinetics were investigated using a graphite furnace atomic absorption spectrometer. The results were analyzed using both pseudo first and second-order models. The molar sorption capacity of WO_3 nanopowder for Pb^{2+} was shown to be 36%. The nature of the starting material in solution was explored by dynamic light scattering (DLS). The morphology of the materials before and after reaction with lead were studied by scanning electron microscopy (SEM) and transmission electron microscopy (TEM), showing the starting materials undergo a large morphological change after the reaction with Pb^{2+}. The material after reacting with excess lead was also characterized by powder X-ray diffraction (XRD) and Raman spectroscopy, showing the formation of crystalline stolzite, $PbWO_4$. Lastly, a cyclic process for the recovery of the sorbent was highlighted for the recovery of the starting material with a very high yield and permitting the toxic heavy metal to be properly disposed.

Introduction

Heavy metal contamination of aqueous systems is not only a problem relating to human health and the environment, but also for the economic issues it presents.[1] The introduction of contaminants into water can occur from natural sources (e.g. leaching from minerals) or human related sources (e.g. industrial effluents). With the rapid development of industries, such as metal plating facilities, mining operations, fertilizer industries, etc., heavy metal wastewaters are increasingly directly or indirectly discharged into the environment, especially in developing countries. Unlike many organic contaminants, heavy metals are not biodegradable and tend to accumulate in living organisms, many of which are known to be toxic and/or carcinogenic.[2]

Human exposure to lead, typically results from lead plumbing materials such as solder and brass fittings, and lead-based paint. Lead exposure has also been associated the release of airborne particulates from industrial or waste elimination emissions and fallout from decades of leaded gasoline emissions.[3, 4] Lead has been found to have acute toxicity when present in drinking water at high amounts. The drinking water guideline recommended by World Health Organization (WHO) is 10 µg/L,[5] while the Environmental Protection Agency (EPA) has a maximum allowance of 15 µg/L.[6]

Department of Chemistry, Oklahoma State University, 107 Physical Sciences, Stillwater, Oklahoma 74078, USA
**Email: allen.apblett@okstate.edu Fax : 405-744-5943*
Tel: 405-744-6007

DOI: 10.1039/x0xx00000x

Materials for the remediation of lead have been extensively studied leading to a very broad range of water treatment options. Treatment processes usually include chemical precipitation,[7, 8] adsorption,[9, 10] solvent extraction,[11-13] ultrafiltration,[14, 15] and ion exchange.[16-18] Many of these processes face shortfalls resulting from low capacity, inadequate affinity, poor effectiveness, high cost, or a combination of these. In addition to the ion-exchange materials referenced above, numerous sorbents have been reported for lead and other heavy metals. These include iron oxides and other metal oxides, fly ash, zeolites, clay minerals, activated carbon, biobased sorbents such as lignin, bark and other tannin-rich materials, chitin, chitosan, seaweed, algae, alginate, xanthated wool and cotton, peat moss, bone char, bagasse, and leaf mould.[19-22] Nanotechnology has shown promise for remediation of lead-contaminated waters due to the high surface area and unusual surface properties of the nanoparticles leading to efficient sorption processes.[19, 23-25]

Apblett *et al.* have demonstrated the attractiveness of using transition metal oxides as water remediation technologies.[26-31] More specifically, they have highlighted the highly reactive nature of molybdenum trioxide towards Pb^{2+} in aqueous systems, showing a very high capacity (110% by weight).[30, 32] However, due to the slight solubility of molybdenum trioxide in water, it is possible that toxicity issues may make the use of MoO_3 unsuitable for the purification of potable water. The similarities in the chemistries of molybdenum and tungsten oxides has led to exploration of whether tungsten oxides are a suitable alternative for MoO_3 as an environmentally friendly sorbent and the results of this investigation are presented herein Notably, WO_3 is insoluble in water and nontoxic making it an attractive alternative for an environmentally friendly

material for Pb^{2+} mitigation. Further, this study will possibly shed light on the eventual fate of nanometric tungsten metal (that eventually turns into tungsten oxide) released into the environment.

Experimental

All chemicals were ACS reagent grade or higher and were used without further purification. Water was purified by reverse osmosis and then deionized to a resistivity of 18 MΩ. Lead nitrate, $Pb(NO_3)_2$ (Sigma-Aldrich), was used to prepare the lead stock solution with a concentration of approximately 100 mg/L. Tungsten (VI) oxide nanopowder [<100 nm (BET)], a commercially-available product from Aldrich, was used as the sorbent for this study. The concentrations of the stock and treated solutions were determined using a Varian GTA120/AA240Z graphite furnace atomic absorption spectrometer (GFAAS) equipped with an auto sampler. A NIST-traceable 100 mg/L Pb^{2+} standard (BDH ARISTAR) was used to prepare the standard solutions used for analysis. Aliquots of the treated samples were taken at regular time intervals and diluted to the appropriate concentrations with a solution of 1% HNO_3, made using trace metal grade HNO_3 from Mallinckrodt.

The surface area of the sorbent was measured by nitrogen physisorption using a NOVA Quantachrome 1200 BET. Scanning electron micrographs of the solids before and after treatment were recorded using a FEI Quanta 600 field emission gun environmental scanning electron microscope. The powders from before and after sorption of Pb^{2+} were embedded, then sectioned with a microtome and imaged by transmission electron microscopy (TEM) on a JEOL JEM-2100 transmission electron microscope. X-ray powder diffraction (XRD) patterns of the sorbent loaded to capacity with lead were obtained on a Bruker D8-A25-Advance equipped with a LynxEye detector. A Raman spectrum of the sorbent after treating the lead solution was recorded on a Nicolet NXR 9610 Raman spectrometer. Determination of the particle size by dynamic light scattering (DLS) and the zeta potential of the solutions were measured using a Brookhaven Instruments Corporation ZetaPALS. A small amount (0.1% by volume) of the electrolyte KCl was added to the samples for the zeta potential measurements.

The effect of sorbent dosage on reaction kinetics was investigated for the nanometric WO_3 material by treating three different 50 mL solutions of 100 ppm Pb^{2+}. For each treatment the amount of tungsten trioxide in excess was varied. The samples were agitated by a sample rotator, at a speed of 40 RPM, to eliminate the possibility of forming concentration gradients. Aliquots of each sample were taken at regular time intervals, diluted with 1% HNO_3 to the appropriate concentration for the analytical instrument, and then analyzed by GFAAS. The reaction uptake curves were plotted using the sorption capacity at a given time (q_t) vs time (t). Sorption capacity was defined by Eq. 1, where C_t is the concentration of analyte in the solution at time t, C_0 is the starting concentration, V is the volume of the analyte, and m is the mass of the sorbent.[33]

$$q_t = \frac{(C_0 - C_t)V}{m}. \quad (1)$$

An uptake capacity study was also performed to determine the maximum uptake of lead by the WO_3 sorbent. Roughly 0.6 g (2.6 mmol) of the WO_3 nanopowder was used to treat a solution containing a large excess Pb^{2+} (50.3 mL of a 0.071 M solution). The sorbent was allowed to react with lead for roughly one month to allow for equilibrium to be established; these solutions were then analyzed to determine the amount of Pb^{2+} removed. Further, all of the solids were characterized by XRD, Raman spectroscopy, SEM, and TEM.

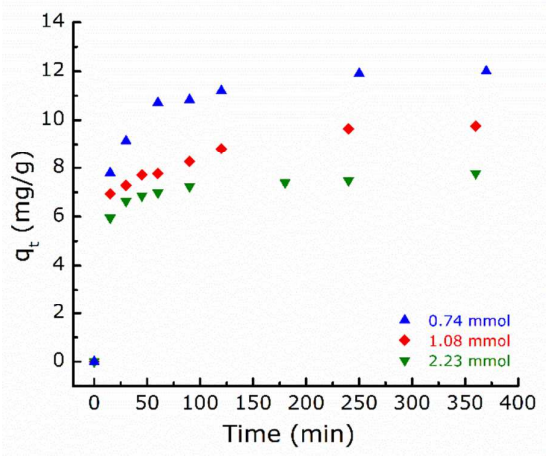

Fig. 1: Sorption uptake curves of Pb^{2+} by nano-WO_3

Results and Discussion

Kinetics

Analysis of the sorbent by N_2 physisorption showed a surface area of 7.5 m^2/g. The sorption uptake curves (Fig. 1) depicts the sorption uptake curve of lead by differing amounts of the sorbent. The data from the uptake curves shows a process in which sorption is initially very fast, then starts to slow as the reaction approaches an equilibrium state. This state occurs at around 100 minutes for the sample treated with 0.743 mmol of WO_3 and roughly 50 minutes when the highest amount of sorbent is used (2.23 mmol WO_3). The sorption process continued at a slow rate until the concentration of the analyte fell below the instrument detection limit of roughly 0.5 ppb.

The uptake kinetics of contaminants by a sorbent is crucial for determining if material can be useful for full-scale batch processes. The kinetics for the sorption process were analyzed using both pseudo first and second-order models, which are commonly used to model sorption processes. The information gained from the kinetic experiments may help to determine if

nanometric tungsten oxide can possibly be incorporated as a sorbent in commercial applications.

The pseudo first-order rate expression was first described by Lagergren (Eq. 2), where q_t is the amount of the analyte sorbed at time t, k_1 is the rate constant of the pseudo first-order sorption process, and q_e is the amount of analyte sorbed at equilibrium.[34]

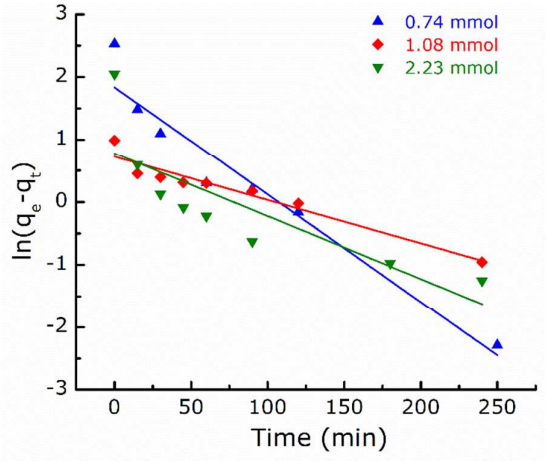

$$q_t = q_e(1 - e^{-k_1 t}) \quad . \qquad (2)$$

Fig. 2: Linear pseudo first-order plot for the uptake of Pb^{2+} by nano-WO_3

Table 1: Kinetic Data from the Linear Pseudo First-order Model of the Uptake of Pb^{2+} by Nano-WO_3

WO_3 (mmol)	k_1 (min^{-1})	q_e (mg/g)	q_e-experimental (mg/g)	R^2
0.74	1.70 x 10^{-2}	6.26	12.6	0.939
1.08	1.59 x 10^{-2}	5.27	9.76	0.936
2.23	1.00 x 10^{-2}	2.17	7.77	0.671

By taking the natural log of Eq. 2, the values of k_1 and q_e can be determined from the linear pseudo first order plot (Eq. 3). The linear plot of $\ln(q_e\text{-}q_t)$ vs. time gives the values of k_1 and q_e from the slope and intercept, respectively. Fig. 2 shows that the linear pseudo first-order kinetic model for the nano-WO_3 did not apply throughout the various sorbent loadings. As the sorbent mass was increased, the data exhibits a large deviation from linearity, as is evident from the R^2 values (Table 1). Furthermore, the estimated values of q_e calculated from the equation differ substantially from those measured experimentally; owing to the fact this sorption process cannot be satisfactorily described by the linear pseudo first-order model. This type of discrepancy has been hypothesized to be due to similar concentrations of solute ions and the reaction sites on the sorbent.[35]

$$\ln(q_e - q_t) = \ln - \frac{k_1}{2.303} t \quad . \qquad (3)$$

Kumar has shown that modeling sorption processes using the nonlinear pseudo first-order model (Eq. 2) was much more appropriate for modeling the sorption of methylene blue on activated carbon.[36] The plotted uptake curves fitted with the nonlinear pseudo first-order equation shows that the model underestimated q_e in all cases (Fig. 3). However, the R^2 values for the nonlinear method were much higher than that of the linear model (Table 2). Also, the q_e values were relatively close to what was observed experimentally as well. These results suggest that this method is far superior to the linearized equation to model this process.

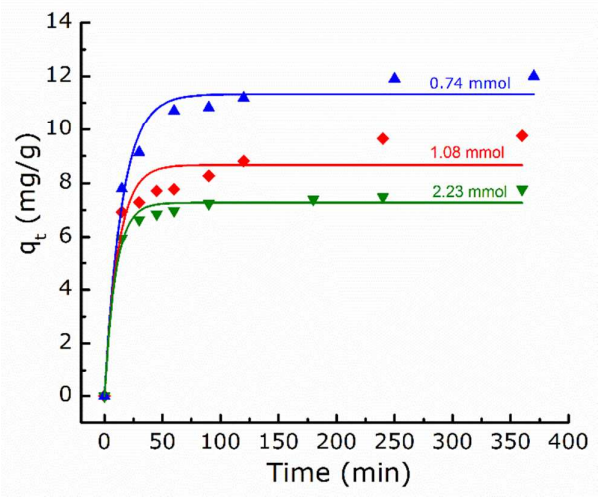

Fig. 3: Nonlinear pseudo first-order fit for the uptake of Pb^{2+} by nano-WO_3

Table 2: Kinetic Data from the Nonlinear Pseudo First-order Model of the Uptake of Pb^{2+} by Nano-WO_3

WO_3 (mmol)	k_1 (min^{-1})	q_e (mg/g)	q_e-experimental (mg/g)	R^2
0.74	6.71 x 10^{-2}	11.3	12.6	0.979
1.08	8.59 x 10^{-2}	8.67	9.76	0.923
2.23	1.05 x 10^{-1}	7.27	7.77	0.984

Ho and McKay proposed a pseudo-second order kinetic model, represented as

$$\frac{t}{q_t} = \frac{1}{k_2 q_e^2} + \frac{1}{q_e} t \quad . \qquad (4)$$

The rate constant (k_2) of the pseudo second-order sorption process has the units g/mg·min, thus is dependent on both the analyte and sorbent.[10] The previous equation can be further simplified by substituting h in place of $k_2 q_e^2$, where h can be considered as the initial sorption rate, as t/q_t approaches 0 (Eq. 5).

$$\frac{t}{q_t} = \frac{1}{h} + \frac{1}{q_e} t \quad . \qquad (5)$$

The slope and the intercept of the plot of t/q_t versus t gives the values of q_e and h, respectively.[35] Using the value of q_e and h, the rate constant (k_2) can be obtained.

The linear pseudo second-order plot for the sorption of lead using nanometric tungsten trioxide had a relatively good fit in all cases (Fig. 4). From the data (Table 3) it is shown that this model fits this sorption process much better than the linear pseudo first-order model. The R^2 values from the linear regression plots for this model were very high (R^2>0.99) and the calculated q_e values were in very close agreement with the

experimental data. The equilibrium concentration (q_e) was only slightly overestimated throughout the series. However, the values of k_2 did not display a correlation with respect to the differing amounts of solid used nor did the values of h. While the linear pseudo second-order model fit the present data very well, there is little physical significance that can be extrapolated from the kinetic results. This is likely due to k_2 being dependent on both the sorbent and analyte. There has,

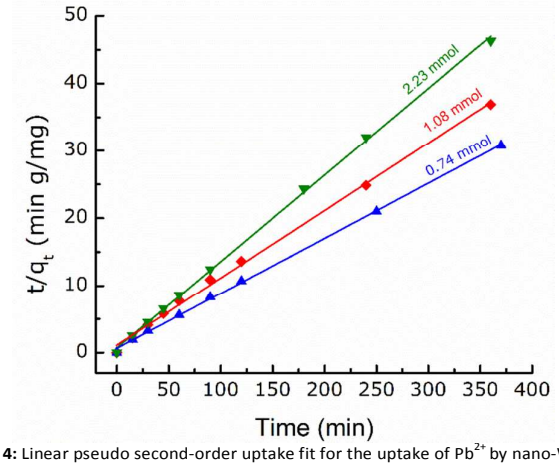

Fig. 4: Linear pseudo second-order uptake fit for the uptake of Pb^{2+} by nano-WO_3

Table 3: Kinetic Data from the Linear Pseudo Second-order Model of the Uptake of Pb^{2+} by Nano-WO_3

WO_3 (mmol)	k_2 (g/mg·min)	h (mg/g·min)	q_e (mg/g)	q_e-exp (mg/g)	R^2
0.743	1.20 x 10^{-2}	1.95	12.8	12.6	0.999
1.08	1.11 x 10^{-2}	1.10	9.98	9.76	0.998
2.23	2.42 x 10^{-2}	1.46	7.78	7.77	0.999

however, been concerns raised on the validity of the linear pseudo second-order model due to a spurious correlation.[29]

The nonlinear pseudo second-order equation was also used for modeling the sorption process, in the form:

$$q_t = \frac{k_2 q_e^2 t}{1+k_2 q_e t}. \quad (6)$$

This equation also effectively modeled the sorption process of methylene blue on activated carbon.[36] The experimental data fit the nonlinear pseudo second-order model with relatively good accuracy (Fig. 5). The R^2 values for the nonlinear method (Table 4) were all very high (>0.97), similar to the linear model, suggesting that this method was also appropriate for modeling this process. As was the case for the linear pseudo second-order model, the kinetic parameters appear to have little physical meaning. The equilibrium concentration values from the model are lower than the experimental values and have larger deviations than the values predicted by the linear pseudo second-order model. From the presented data it can be concluded that the nonlinear pseudo first-order model is the best-suited model determining a rate constant with a physical meaning. However, the linear pseudo second-order model was the most superior in predicting the equilibrium concentrations for the plotted data.

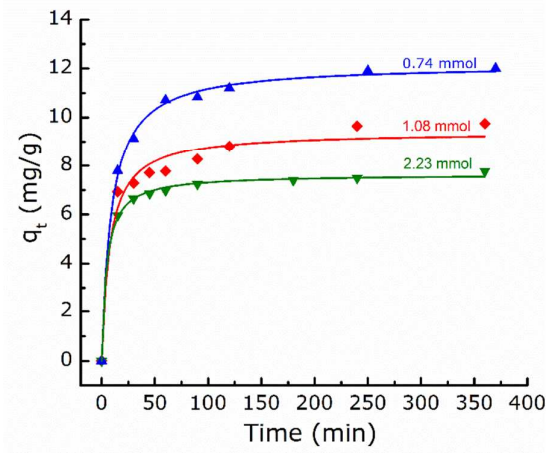

Fig. 5: Nonlinear pseudo second-order fit for the uptake of Pb^{2+} by nano-WO_3

Table 4: Kinetic Data from the Nonlinear Pseudo Second-order Model of the Uptake of Pb^{2+} by Nano-WO_3

WO_3 (mmol)	k_2 (g/mg·min)	h (mg/g·min)	q_e (mg/g)	q_e-exp (mg/g)	R^2
0.743	9.12 x 10^{-3}	1.35	12.2	12.6	0.998
1.08	1.41 x 10^{-2}	1.25	9.42	10.6	0.991
2.23	2.89 x 10^{-2}	1.69	7.64	7.77	0.998

Characterization

Dynamic light scattering (DLS) was used to determine the size of the sorbent in solution. The DLS experiment indicated that the particles were in an aggregated state, with an average particle size of 170.8 nm ± 0.8 nm. The polydispersity of the material suspended in H_2O was very low, 0.084 ± 0.025 nm, suggesting that most of the particles in the solution had similar hydrodynamic radii. The Zeta potential was measured to determine if the aggregates were stable in solution. Nano-particles in solution are said to be stable if the value of the zeta potential is above an absolute value of 30 mV.[31] The zeta potential measurement confirmed that the sorbent was in a stable aggregation state, with an absolute value of 50.44 ± 0.67 mV, with a solution pH of 5.3. The electrophoretic mobility of the solution was -3.94 ± 0.05 µm·cm/V·s.

The sorption capacity of the material was determined by reacting the WO_3 sorbent with excess Pb^{2+}, yielding a 36% molar uptake of Pb^{2+} from the solution. The initial pH of the stock solution was 3.9 and it dropped to 1.1 during treatment. The drop in pH is due to the formation of $PbWO_4$ with the concomitant production of two molar equivalents of protons per formula unit,

$$WO_3 + Pb^{2+} + H_2O \rightarrow PbWO_4 + 2H^+. \quad (7)$$

The large drop in pH possibly affected both the sorption rate and capacity of the material.[37] In this case, however, it is unlikely that the drop in pH affected the sorption kinetics models, since the data fit the models with high R^2 values. The materials isolated from the molar capacity experiment were characterized using Raman, XRD, SEM, and TEM.

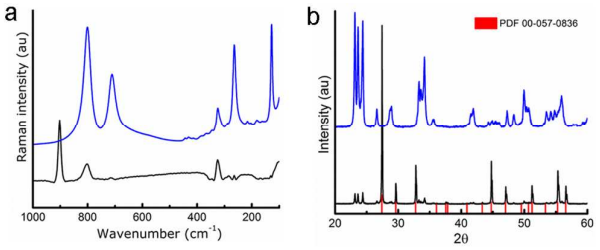

Fig. 6: The Raman spectrum of the nanometric tungsten oxide product after the reaction of WO_3 nanopowder with excess Pb^{2+} (a) and the diffraction pattern of the same material (b). The upper blue spectra are those for the nano-WO_3. The product's (lower black) spectra show characteristics of a newly formed stolzite phase.

The Raman spectrum of the WO_3 nanopowder after reaction with lead (Fig. 6a) showed characteristic stretches for both WO_3 and $PbWO_4$ in the stolzite phase. The symmetric stretching band, $\nu_1(A_g)$, for the tetrahedral tungstate ion in $PbWO_4$ appears at 902 cm^{-1}. The $\nu_2(A_g)$ vibration for stolzite was observed as a strong band at 325 cm^{-1}, however, the weak $\nu_2(B_g)$ band, normally present at 356 cm^{-1} was not resolved in this spectrum.[38-40] The stretches observed at 802 and 716 cm^{-1} are consistent with the ν(O-W-O) vibrational mode of WO_3. Note that these are very strong in the Raman spectrum of the WO_3 nanomaterial (6a). The weak stretching observed at 284 cm^{-1} is most likely resultant of the δ(O-W-O) band.[41]

The X-ray diffraction pattern (Fig. 6b) of the material saturated with lead confirms the formation of the stolzite phase. Along with presence of $PbWO_4$, the pattern also shows the presence of the parent WO_3 material, as can be seen by comparison to the diffraction pattern for the starting material shown in Figure 6b. This is expected since the reaction only proceeds to 36% consumption of WO_3. The materials were identified using the Powder Diffraction Files from the International Centre for Diffraction Database.

The morphologies of the sorbents before and after sorption were characterized using scanning electron microscopy. The micrographs of the WO_3 nanopowder showed the material was comprised of globular and spherical aggregates of nanoparticles (Figure 7a), with diameters ranging from roughly 1 to 5 µm. A close up image of the sorbent shows the nanoparticles that make up the aggregates (Fig. 7b).

The scanning electron micrographs of the material after treatment with lead (Fig. 7c and 7d) showed a major morphology change, from spherical aggregates to larger faceted particles, including octahedrally-shaped particles (Fig. 8c). The markedly different morphologies can be rationalized due to the deconstruction of the WO_6 octahedra in WO_3 to create the WO_4 tetrahedra found in stolzite. Furthermore, the micrograph at 50,000x magnification (Fig. 7d) appears to show that the newly formed particles are not large aggregates of nanoparticles, but single monoliths with nanoparticles decorating the surface. The newly formed material shows an obviously large size increase with an average diameter of particle of 3.93 ± 1.24 µm (n = 31).

The particle size of the starting and treated materials were analyzed by TEM, using thin sections of embedded material. The average particle size for the starting materials was 27 ± 14 nm (n = 75). After the materials were treated with excess Pb^{2+}, the particles were larger, with an average size of 35 ± 31 nm (n = 75). The largest particle measured for the treated sample was 157 nm and the smallest particle was only roughly 7 nm. Measurements were also made by suspending the particles in acetone and dropping them onto a TEM grid. The results from this experiment were fairly consistent with the sectioned untreated material, with an average particle size of 22 ± 11 nm (n = 57). Notably, the width of the diffraction lines of the XRD pattern (Fig. 6b) calculated using the Pearson VII function (corundum reference) and the Scherrer equation was 36.6 nm. This value is in good agreement with the TEM values suggesting the observed particles are single grains. TEM characterization of suspensions of the treated material, showed a significantly larger average particle size than the sectioned material. The particles had an average size of 51 ± 69 nm (n = 75). The largest particle from the treated material was roughly 450 nm, with the smallest measuring only 5 nm. This result could be due to the sectioning procedure for the larger particles leading to results for the diameter, rather than the length of the rod-like particles like the one shown in Fig. 8c. The treated material also showed lattice fringes corresponding to the (111) plane of stolzite (Fig 8d).

The results from the TEM experiments are consistent with the observations from SEM that there is a formation of larger particles during reaction with Pb^{2+}. The formation of the large monoliths decorated with small particles on the surface was observed in both the SEM and TEM images (Figs. 7d and 8c). The size of the smaller particles are consistent with what was observed for the starting material. It is possible the small particles observed were consequence of unreacted starting material, since only 36% of the WO_3 was transformed into $PbWO_4$.

Recovery of the Sorbent

To showcase the ability for the material to be recycled, $PbWO_4$ was synthesized by a precipitation reaction of $Pb(NO_3)_2$ with $Na_2WO_4 \cdot 2H_2O$ followed by calcination of the precipitate at 600 °C. X-ray powder diffraction showed that the product was phase-pure stolzite. The regeneration-cycle (Fig. 9) features a reaction of $PbWO_4$ with excess 30% NH_4OH, yielding an insoluble lead hydroxide product and soluble ammonium tungstate that can readily be separated by filtration. The filtrate was evaporated to dryness and the resulting powder was calcined at 550 °C to generate a WO_3 in a 99% yield.

Fig. 7: SEM micrographs of nano-WO_3 at (a) 5,000x and (b) 50,000x magnification and the material after treating Pb^{2+} at (c) 5,000x and (d) 50,000x magnification

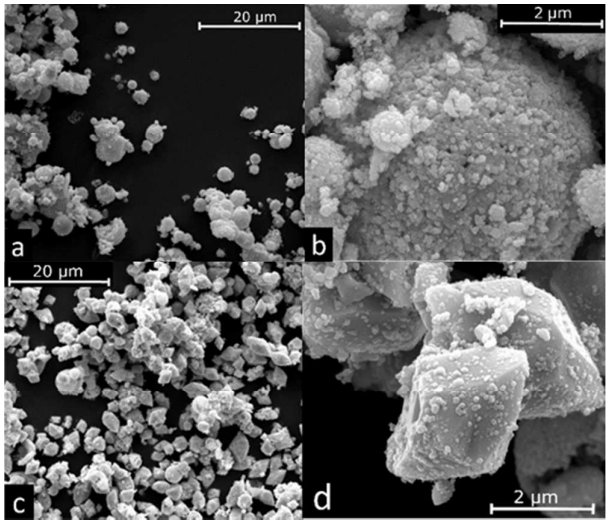

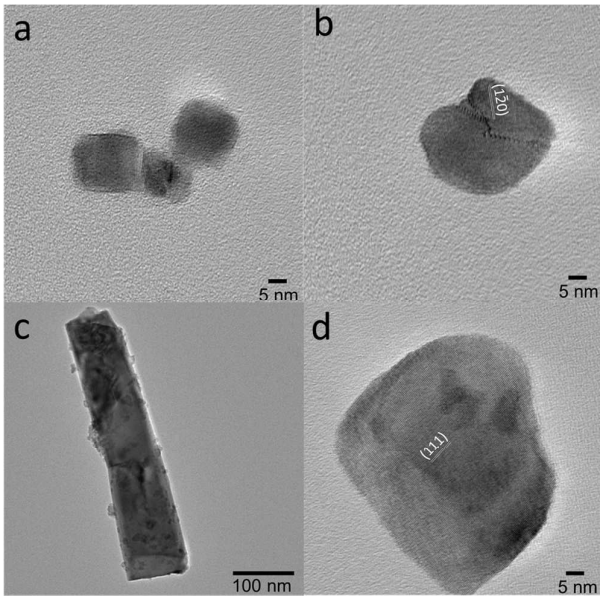

Fig. 8: TEM micrographs of from the material suspended in acetone. The nano-WO_3 (a and b) shows fairly uniform small particles, with lattice fringes due to the $(1\bar{2}0)$ plane of WO_3 highlighted in b. The material after treating excess Pb^{2+} (bottom) show much larger particle sizes and lattice fringes characteristic of the (111) plane of stolzite.

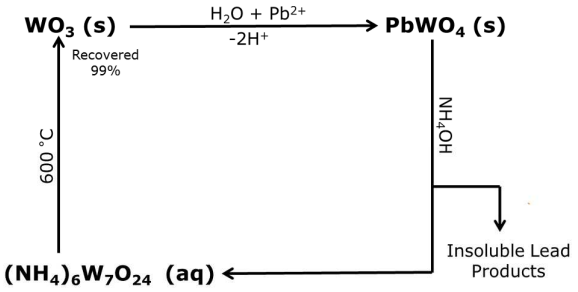

Fig. 9: Cyclic-green process for recovery of the WO_3 sorbent

Conclusion

The results from this study show that commercially available tungsten trioxide nanopowder is an attractive material for the remediation of aqueous lead. The study provides a potential material to be rapidly incorporated into current treatment processes since the material is already commercially available. The material may also show an increased capacity and reaction kinetics when tested in a buffered system, as pH has been shown to affect sorption. Furthermore, this process is not only attractive due to the non-toxic nature of the starting material, but because the spent materials can be easily separated from the solution and recycled in a green fashion. The reaction with Pb^{2+} produced $PbWO_4$ crystals with interesting morphologies, with the stolzite structure as demonstrated by XRD and Raman spectroscopy. Modeling of the sorption process gave reasonable results using both the linear and nonlinear pseudo-second order equations. The linear pseudo first-order model was not appropriate to model any of the sorption processes and the nonlinear pseudo first-order model was much more effective.

Notes and references

1. J. E. Marcovecchio, S. E. Botte and R. H. Freije, in *Handbook of Water Analysis*, ed. L. M. L. Nollet, CRC Press, London, 2 edn., 2007, ch. 11
, pp. 275-311.
2. F. L. Fu and Q. Wang, *J Environ Manage*, 2011, **92**, 407-418.
3. T. Abdel-Fattah and K. B. Payne, *Journal of Environmental Science and Health Part A* 2004, **227**, 2275-2291.
4. D. A. Burgoon, S. W. Rust and K. A. Hogan, in *Lead Poisoning Exposure, Abatement, Regulation*, ed. J. J. Breen, Stroup, C.R., Lewis Publsihers Boca Raton, 1995, pp. 255–264.
5. Y. Sayato, *Eisei Kagaku*, 1989, **35**, 307-312.
6. E. P. Agency, 2009, 1-6.
7. M. M. Matlock, B. S. Howerton and D. A. Atwood, *Industrial & Engineering Chemistry Research*, 2002, **41**, 1579-1582.
8. J. O. Esalah, M. E. Weber and J. H. Vera, *The Canadian Journal of Chemical Engineering*, 2000, **78**, 948-954.
9. R. M. McKenzie, *Soil Research*, 1980, **18**, 61-73.
10. Y.-S. Ho and G. McKay, *Process Biochemistry*, 1999, **34**, 451-465.
11. J. G. Dean, F. L. Bosqui and K. H. Lanouette, *Environmental Science & Technology*, 1972, **6**, 518-522.
12. K. Bang Mo, *Journal of Membrane Science*, 1984, **21**, 5-19.
13. J. Pichtel and T. M. Pichtel, *Environmental Engineering Science*, 1997, **14**, 97-104.
14. F. Ferella, M. Prisciandaro, I. De Michelis and F. Veglio, *Desalination*, 2007, **207**, 125-133.
15. K. E. Geckeler and K. Volchek, *Environmental science & technology*, 1996, **30**, 725-734.
16. M. Trgo, J. Perić and N. V. Medvidović, *Journal of Hazardous Materials*, 2006, **136**, 938-945.

17. V. K. Gupta and I. Ali, *Journal of Colloid and Interface Science*, 2004, **271**, 321-328.
18. V. K. Gupta, M. Gupta and S. Sharma, *Water Research*, 2001, **35**, 1125-1134.
19. M. T. Amin, A. A. Alazba and U. Manzoor, *Advances in Materials Science and Engineering*, 2014, **2014**, 24.
20. S. E. Bailey, T. J. Olin, R. M. Bricka and D. D. Adrian, *Water Research*, 1999, **33**, 2469-2479.
21. G. Zhao, X. Wu, X. Tan and X. Wang, *The Open Colloid Science Journ*, 2010, **4**, 19-31.
22. J. He and J. P. Chen, *Bioresource Technology*, 2014, **160**, 67-78.
23. M. Hua, S. Zhang, B. Pan, W. Zhang, L. Lv and Q. Zhang, *Journal of Hazardous Materials*, 2012, **211–212**, 317-331.
24. X. Wang, Y. Guo, L. Yang, M. Han, J. Zhao and X. C., *J Environ Anal Toxicol*, 2012, **2:154**.
25. P. Xu, G. M. Zeng, D. L. Huang, C. L. Feng, S. Hu, M. H. Zhao, C. Lai, Z. Wei, C. Huang, G. X. Xie and Z. F. Liu, *Science of The Total Environment*, 2012, **424**, 1-10.
26. H. Albusaidi and A. W. Apblett, in *Environmental Issues and Waste Management Technologies in the Materials and Nuclear Industries XII*, John Wiley & Sons, Inc., 2009, DOI: 10.1002/9780470538371.ch5, pp. 39-46.
27. K. N. Barber and A. W. Apblett, *Ceramic Transactions*, 2009, **207**, 171-175.
28. M. Chehbouni, H. Al-Busaidi and A. W. Apblett, in *Nuclear Energy and the Environment*, American Chemical Society, 2010, vol. 1046, ch. 13, pp. 155-167.
29. B. P. Kiran and A. W. Apblett, *Ceramic Transactions*, 2004, **155**, 371-380.
30. B. P. Kiran, A. W. Apblett and M. M. Chehbouni, *Ceramic Transactions*, 2003, **143**, 385-394.
31. A. W. Apblett, B. P. Kiran and M. Chehbouni, *Ceramic Transactions*, 2006, **176**, 15-23.
32. C. K. Perkins, K. N. Barber and A. W. Apblett, *CrystEngComm*, 2014, DOI: 10.1039/C3CE42221F.
33. C. Dwivedi, S. K. Pathak, M. Kumar, S. C. Tripathi and P. N. Bajaj, *RSC Advances*, 2013, **3**, 22102-22110.
34. S. Lagergren, *Handlingar*, 1898, **24**, 1-39.
35. S. Azizian, *Journal of Colloid and Interface Science*, 2004, **276**, 47–52.
36. K. V. Kumar, *Journal of Hazardous Materials B*, 2006, **137**, 1538-1544.
37. K. S. Smith, *Reviews in Economic Geology* 1999, **6A-B**, 161-182.
38. R. K. Khanna, W. S. Brower, B. R. Guscott and E. R. Lippincott, *Journal of Research of the National Bureau af Standards - A*, 1968, **72A**, 81-84.
39. B. Ingham, S. V. Chong and J. L. Tallon, *The Journal of Physical Chemistry B*, 2005, **109**, 4936-4940.
40. S. Bastians, G. Crump, W. P. Griffith and R. Withnall, *Journal of Raman Spectroscopy*, 2004, **35**, 726-731.
41. M. F. Daniel, B. Desbat, J. C. Lassegues, B. Gerand and M. Figlarz, *Journal of Solid State Chemistry*, 1987, **67**, 235-247.